Chemical Science

ROYAL SOCIETY OF CHEMISTRY

PERSPECTIVE

View Article Online
View Journal | View Issue

Cite this: *Chem. Sci.*, 2020, **11**, 6606

All publication charges for this article have been paid for by the Royal Society of Chemistry

Received 10th May 2020
Accepted 13th June 2020

DOI: 10.1039/d0sc02658a

rsc.li/chemical-science

Carbon-based antiviral nanomaterials: graphene, C-dots, and fullerenes. A perspective

Plinio Innocenzi * and Luigi Stagi *

The appearance of new and lethal viruses and their potential threat urgently requires innovative antiviral systems. In addition to the most common and proven pharmacological methods, nanomaterials can represent alternative resources to fight viruses at different stages of infection, by selective action or in a broad spectrum. A fundamental requirement is non-toxicity. However, biocompatible nanomaterials have very often little or no antiviral activity, preventing their practical use. Carbon-based nanomaterials have displayed encouraging results and can present the required mix of biocompatibility and antiviral properties. In the present review, the main candidates for future carbon nanometric antiviral systems, namely graphene, carbon dots and fullerenes, have been critically analysed. In general, different carbon nanostructures allow several strategies to be applied. Some of the materials have peculiar antiviral properties, such as singlet oxygen emission, or the capacity to interfere with virus enzymes. In other cases, nanomaterials have been used as a platform for functional molecules able to capture and inhibit viral activity. The use of carbon-based biocompatible nanomaterials as antivirals is still an almost unexplored field, while the published results show promising prospects.

1. Introduction

The Covid-19 viral infection, which has become one of the most significant threats to human health since the 1918 flu pandemic, has urgently increased the need for antiviral drugs and vaccines. The times required to develop them are, however, quite long and several phases are required before being approved for use in humans. As a result, it is important to develop innovative and long-term strategies to complement the existing pharmacological approaches to fight infections and specific viruses. Despite the great advances in technology, human beings often find themselves helpless in the face of new dangers arising from the emergence of new viruses. Viruses are the cause of about one third of deaths from infectious diseases.[1] The lack of tools to fight virulent infections or a slow response to the outbreak of a pandemic can have catastrophic economic and social implications. Unfortunately, the only resource to counteract the development of viral infections is the use of vaccines, often employed when the infection is already widespread. Besides that, the few strategies we possess are antiviral drugs, symptom treatment, and isolation. Beyond the urgency to reduce and stop the pandemic, it is also necessary to develop a new generation of antiviral tools that are as flexible as possible and show broad range antiviral activity. Viruses are characterized by well-defined shapes and dimensions, which are in the nanoscale, and as such they could also be considered as a kind of nanomaterial themselves. Highly symmetric nanostructures, such as fullerenes, have, for instance, extraordinary geometric affinity with icosahedral viruses.[2] The possibility of creating nanomaterials on the same scale and with similar geometry is a fascinating possibility. The similarities can be used to foster interactions and build smart nanostructures that can inhibit or inactivate virus replication.

Antiviral substances can generally be divided into virostatic and virucidal, depending on the counteracting action against a particular virus.[1] The former are substances that act in the early stages of infection by inhibiting viral replication and the proliferation of the virus. They are based on a binding mechanism and can, therefore, often be ineffective if they detach and leave the viral particles untouched.[1] Virucidal medicines, on the other hand, can permanently deactivate the virus, with effects that remain even after dilution. However, many of the molecules that have such an effective antiviral action are toxic.[1] Research on the antiviral properties of carbon-based nanomaterials is still in its embryonic state. The main interest in these systems lies precisely in their potential low toxicity[3] and innovative virus inhibition mechanisms. The ambition of using nanoscale systems is to combine virostatic properties with virucidal inactivation processes.

Among the nanomaterials that have been tested in nanomedicine and biotechnology, nanoparticles are certainly the most important to date.[4–6] Their antiviral activity is exerted through multiple mechanisms. The small size and tailored functionalization of the surface favour drug delivery and entry

Department of Chemistry and Pharmacy, Laboratory of Materials Science and Nanotechnology, CR-INSTM, University of Sassari, via Vienna 2, Sassari, 07100, Italy. E-mail: plinio@uniss.it; lstagi@uniss.it

through the cell membrane (negatively charged). They can also have biomimetic properties as in the case of dendrimers.[1] The possibilities of using nanomaterials for nanomedical purposes are potentially vast and take advantage of the flexible synthesis, biocompatibility, surface tunability, and design of the chemical and structural composition.[4]

In this perspective review, we have considered the most significant results in the field of carbon-based nanomaterials for antiviral applications. In general, carbon nanomaterials show low cytotoxicity and present specific antiviral activities. Although relatively new in the nanomedical field, they have stimulated intense research activity aimed at controlling the synthesis and functionalization of their surfaces. The related surface engineering has allowed effective tuning of the surface properties for specific applications. Graphene-based systems have proven to work well both *via* direct interaction with the virus (also through photo-induced mechanisms) and as platforms for other particles or molecules with antiviral properties. In addition to graphene, carbon dots, systems smaller than 10 nm, have also been shown to have specific antiviral properties and broad-spectrum responses. The other class of carbon nanomaterials that we have considered is fullerene and its derivatives. They were the first ones to be tested as antiviral carbon materials and have shown remarkable antiviral properties as an inhibitor of viral activity or as a photoactivator. It can be envisaged that in the future, the need for antiviral materials will attract more attention towards carbon-based nanomaterials and new fields of application can be expected to be developed.

2. Interaction of viruses and graphene

Application of graphene nanomaterials has been largely exploited in several fields, from electronics to sensing and photonics, but only to a minor extent in nanomedicine.[7] Graphene and graphene oxide have been used as anti-bacterial agents, and for drug or gene delivery,[8] cancer therapy,[9] engineering stem cells,[10] tissue engineering,[11] biosensing[12] and bioimaging.[13]

In particular, graphene oxide has shown antibacterial activity, although a clear origin of this effect has not yet been identified.[14,15] The antibacterial activity of graphene oxide (GO) and reduced graphene oxide (rGO) has been tested on *E. coli* bacteria. It has been observed that GO produces damage to the membranes of bacterial cells, causing the exit of the cytoplasm. It has also been observed that *E. coli* cells respond to GO or rGO exposure in a different way. The *E. coli* cells are singularly wrapped by GO layers, while in the case of rGO they are embedded into large aggregates. GO shows, in general, the highest antibacterial activity, which depends on time and concentration. The origin of this effect has been attributed to oxidative stress. In fact, GO and rGO oxidize glutathione, which acts as the redox state mediator in bacteria, and physically disrupt the membrane *via* direct contact with the sharp parts of the GO layers.[16]

2.1 Direct antiviral activity

The antibacterial activities of GO and rGO sheets suggest that these nanomaterials could also have a direct antiviral action. An evaluation of this activity has been performed using RNA (*porcine epidemic diarrhoea virus*, PEDV)[17] and DNA (*pseudorabies virus*, PRV) viruses as a model.[18] PEDV is a coronavirus that infects pigs causing severe diarrhoea and dehydration, which results in significant mortality in piglets. PEDV cannot be transmitted to humans. PRV is, instead, a herpesvirus of swine, belonging to the *Alphaherpesvirinae* subfamily, which causes Aujesky's disease. Both of these viruses are responsible for worldwide severe economic losses.[19]

Fig. 1 shows the antiviral effect of graphene oxide at noncytotoxic concentrations. Experiments have shown that GO inactivates the virus before it enters the cells. The virus is inactivated by physical disruption of the structure through direct interaction with the sharp edges of the GO layers. Images taken by TEM have shown that the glycoprotein spikes in the virion envelop, after incubation with GO for one hour, have been destroyed. The antiviral activity was effective on both DNA and RNA viruses, and dependent on concentration and incubation time. Interestingly, it has been observed that rGO and GO show a similar antiviral activity, which suggests a minor role of the surface functional groups. Because GO and rGO have a similar negative charge and layered structure, the physical interaction of the viruses with their sharp edges should be at the origin of the antiviral activity. GO has been found to inactivate the virus before it enters the cell. Another important factor is the negative charge of GO, which favours electrostatic interaction with the positively charged viruses. The higher interactions result in the destruction and inactivation of the virus.

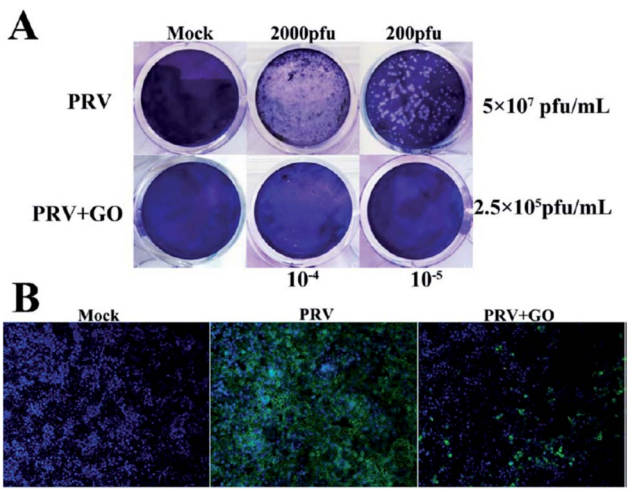

Fig. 1 Anti-PRV activity of graphene oxide on PK-15 cells. (A) Plaque-reduction assay using PK-15 cells infected with PRV in the presence and absence of GO. The number of plaques (clear spots) represents the amount of virus in a given dilution. Mock infected cells (top left); cells infected with PVR of 2000 pfu (top middle) and 200 pfu (top right); cells treated with 6 μg mL^{-1} GO (bottom left); PRV-infected cells in the presence of GO at 2000 pfu (bottom middle) and 200 pfu (bottom right). (B) Indirect immunofluorescence assay of PK-15 cells infected with PRV in the presence and absence of GO. Blue, DAPI; green, FITC-conjugated goat anti-mouse antibody. Reproduced with permission from ref. 18. Copyright 2015 American Chemical Society.

A confirmation of the role of the negative charge of GO can be found in the experiments performed by Sametband *et al.*[20] They tested the antiviral activity of GO layers and partially reduced sulfonated GO (rGO-SO_3). Both of these nanomaterials have a negative charge, due to carbonyl and sulfonate surface groups, and can inhibit the infection from the herpes simplex virus type-1, HSV-1 (*Human Alphaherpesvirus* 1) (*vide infra*). HSV-1 is a double-stranded DNA virus, and is a member of the Human Herpesviridinae family. It is an enveloped virus with a spherical pleomorphic structure whose diameter is around 200–250 nm. HSV-1 causes oral herpes or cold sores in a large portion of the world population.

GO has also been tested as a label free nanomaterial to detect and inhibit viral activity.[21] Two enteric viruses have been used, H9N2 (*endemic gastrointestinal avian Influenza A virus*) and EV71, a virus responsible for hand, foot and mouth disease. H9N2 is a subtype of the *Influenza A virus* (bird flu) belonging to the *Orthomyxoviridae* family. EV71 is a non-enveloped virus of small dimensions, about 30 nm in diameter, belonging to the *Picornaviridae family*. The antiviral effect of GO has been found to be strongly dependent on the temperature; at 25 °C and 37 °C only a weak antiviral activity is detected, less than 0.5 and 1 log respectively (Fig. 2). Experiments have been performed in the presence of GO at 56 °C, a threshold value for virus inactivation.

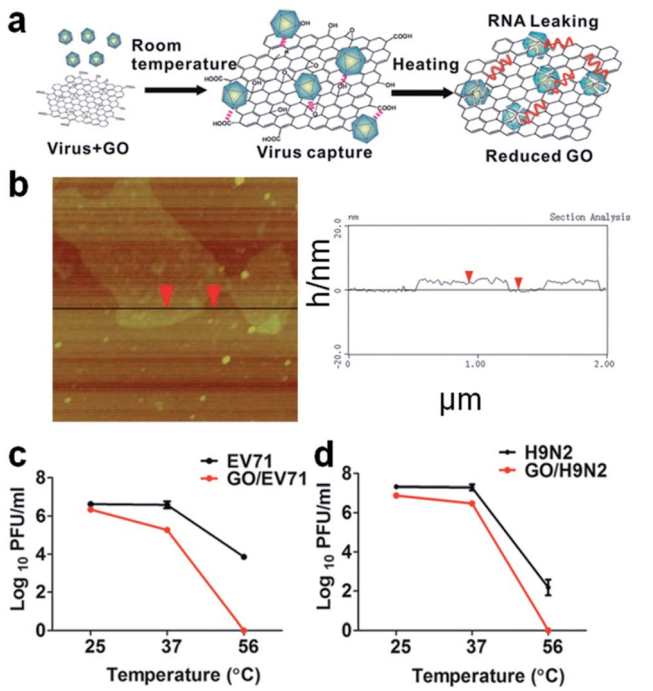

Fig. 2 (a) Schematic representation of the GO and virus interaction exposed at different temperatures. The physiochemical interactions between viruses and reactive oxygenated groups are indicated by dotted lines. The release of viral RNA is described in red. (b) AFM images (left) and height profile (right) of the GO. (c) The temperature-dependent removal of EV71 and (d) H9N2 at room temperature (25 °C), physiological temperature (37 °C), and the commonly used inactivation temperature of viruses (56 °C). Reproduced with permission from ref. 21. Copyright 2014 WILEY-VCH Verlag GmbH & Co. KGaA, Weinheim.

In general, not all viruses inactivate at 56 °C, but both the H9N2 and EV71 viruses lost their infectivity completely when GO was added.

The authors have underlined that the localized reactive oxygen groups on the GO surface are a critical parameter to control the virus binding through the physicochemical reactions activated by the thermal reduction. The viruses captured by GO have shown a loss of structural integrity with destruction of the spike structures. Because of the virus integrity loss, an immediate leaking of RNA is observed. This can be used as a process to extract RNA and for quick virus detection using a one-step RT-PCR assay assisted by GO. After 30 min at 56 °C, the content of leaked RNA in the presence of GO was 46.9% for EV71 and 53% for H9N2, and only 5.6% and 6% without GO.

The direct effect produced by graphene sheets on Ebola virus has also been theoretically investigated. Molecular dynamic calculations have been used to simulate the interactions of graphene with Ebola VP40 oligomers.[22] The graphene layers are able to recognize and break the hydrophobic protein–protein interactions in the matrix protein VP40.

2.2 Antiviral activity through photocatalysis

Another way to inhibit the virus activity using GO is through photocatalysis. GO has a photocatalytic activity[23] which can also be exploited for inhibition of virus activity. To achieve consistent photodegradation, the virus should stay close to the GO surface under UV irradiation. This type of strategy has been developed by Hu *et al.* to synthesise graphene oxide-aptamer nanosheets.[24] The aptamers attached on the GO surface have been used to capture *MS2 bacteriophage viruses*.[25] *MS2 bacteriophage* is a small (23–28 nm) icosahedral non-enveloped RNA virus, which infects the bacterium *Escherichia coli*. Because of its characteristics, it can be used as a model for testing the antiviral properties of GO upon illumination with UV light (Fig. 3). In this case the breakage of the virus protein capsid is predominant with respect to the physical disruption produced by the sharp edge of the GO layers.

In another example, GO layers have been used to produce a GO–Tungsten oxide composite whose antiviral activity has been tested under UV light irradiation using a MS2 bacteriophage virus on the surface of the material.[26]

2.3 Graphene oxide – silver nanoparticle systems

Silver nanoparticles (AgNPs) have shown, in different conditions, a remarkable antiviral activity[27] and in combination with GO, an enhanced antibacterial activity.[28,29] The main mechanism of virus inhibition by AgNPs is physical binding *via* the glycoprotein. The dimensions of the particles are a crucial parameter since size-dependent interactions with HIV-1 viruses have been found only in the 1–10 nm range. The AgNPs preferentially interact with the virus through binding to the glycoprotein. The virus bound to the nanoparticles is no longer able to penetrate the cells.

This peculiar property of AgNPs can be integrated with GO, which acts as a platform for the nanoparticles; this has the advantage of avoiding the agglomeration of the AgNPs while the

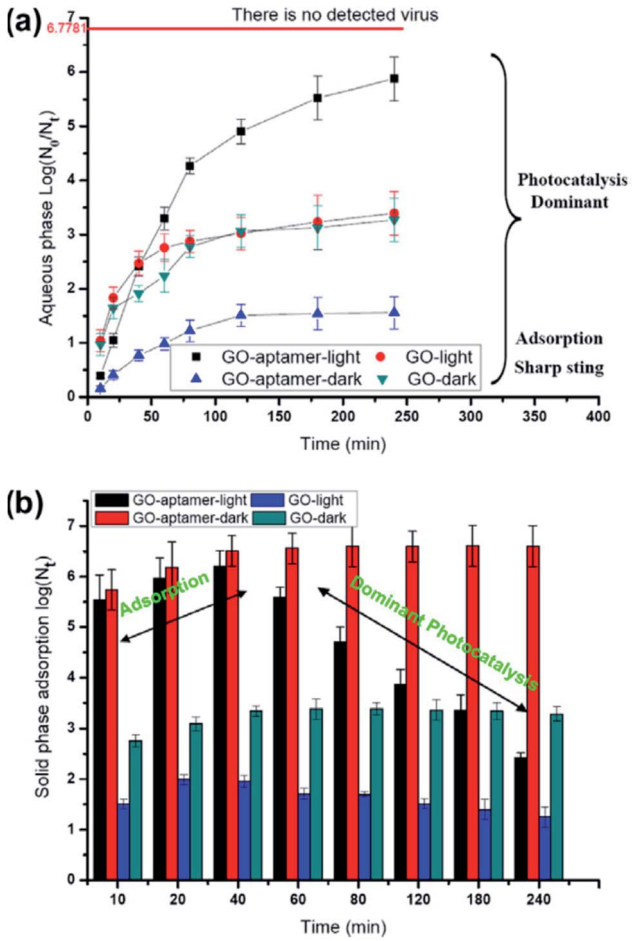

Fig. 3 Survival of viruses in the aqueous phase (a) and solid phase (b) with visible-light irradiation or under dark conditions. The line of no detected viruses expresses only one virus in the suspension. Reproduced with permission from of ref. 24. Copyright 2012 Elsevier Ltd.

negatively charged GO may attract the virus. The therapeutic approach is based on using the NPs as an extracellular inhibitor, preventing the viruses from entering the cells. The antiviral activity of a GO–AgNPs nanocomposite has been tested with non-enveloped viruses, *feline coronavirus* (FCoV) and *infectious bursal disease virus* (IBDV).[30] The non-enveloped FCoV belongs to the family of *Coronaviridae* and species *Alphacoronavirus 1*. It infects cats worldwide and is responsible for the most common and deadly feline infectious diseases. IBDV is a double-stranded RNA non-enveloped virus of the *Birnaviridae* family and *Infectious Bursal disease species* with a diameter of 60–65 nm. Only a limited antiviral activity has been detected; in the best case, the GO–Ag nanosystem was able to inhibit 25% of infection by FCoV.

A similar approach has been followed by Du *et al.*, to prevent viral entry into the cells.[31] AgNPs have been self-assembled on the surface of GO *via* interfacial electrostatic forces. The inhibition efficiency was 59.2% in the case of porcine reproductive and respiratory syndrome virus (PRRSV), which is an RNA virus with a strong impact on the pig industry (Fig. 4). Interestingly, besides the antiviral effect due to the virus binding with the AgNPs, another mechanism has been suggested. The GO–AgNPs enhance the production of interferon-α (IFN-α) and IFN-stimulating genes (ISGs), which causes direct inhibition of virus proliferation.

2.4 Mimicking the cell surface

Another extracellular route to inhibit the virus activity is using GO layers as a platform to mimic the cell surface receptors. GO derivatives, obtained by binding on the nanosheet surface heparan sulphate (HS), have been shown to compete with HSV-1.[20] HS is a linear polysaccharide which is negatively charged. HSs are attached to the cell surface as proteoglycans (HPGs) and may become cellular receptors for different viruses. To mimic the surface of the cell, GO layers have been functionalized by sulfonated groups (GO-SO_3), as previously discussed.[20]

Other examples that mimic the extracellular cell matrix have been reported, which include GO functionalization with polyglycerol sulfate,[32] β-cyclodextrin[33] and polyglycerol sulphate in combination with alkyl chains.[34]

A main issue regarding the functionalization of GO is controlling the density and distribution of the groups attached to the surface. Gholami *et al.*[35] developed a one-pot [2 + 1] nitrene cycloaddition reaction to functionalize graphene by 2-azido-4,6-dichloro-1,3,5-triazine (Fig. 5). In a second step, the GO surface was covered with sulphonate groups using polyglycerol with a few amino functional groups, $PG(NH_2)_{4\%}$. This method allowed a platform with a uniform distribution of hyperbranched polyglycerol on the surface to be obtained. In a further step, the surface was sulphated to obtain a heparin sulphate mimetic 2D material. The nanoplatform is highly negatively surface charged and has a very good dispersibility in an aqueous environment. The capability of this platform to bind viruses has been tested using *Vesicular Stomatitis Virus* (VSV) as a model. VSV is an enveloped virus belonging to the *Rhabdoviridae* family and *Indiana vesicolorum* species. It is a zoonotic virus which is commonly used for laboratory studies of viral evolution in *Rhabdoviridae* viruses.

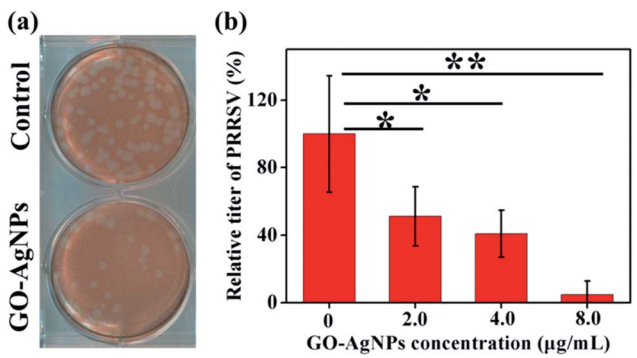

Fig. 4 Effect of GO-AgNP nanocomposites on the entry of PRRSV. (a) Plaque assays of the control and PRRSV before exposure to 4.0 μg mL^{-1} GO–AgNP nanocomposites. (b) The influence of the concentration of the GO–AgNPs nanocomposites on the relative titer of the virus. Reproduced with permission from ref. 31. Copyright 2018 American Chemical Society.

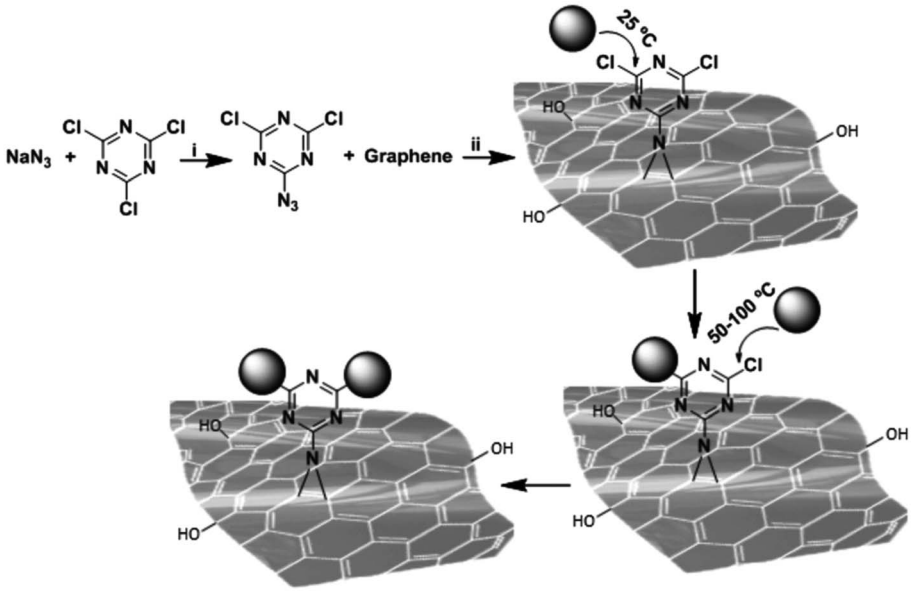

Fig. 5 Functionalization of graphene by [2 + 1] nitrene cycloaddition using 2-azido,4,6-dichloro-1,3,5-triazine as a nitrene precursor. Stepwise nucleophilic substitution of chlorine atoms of triazine groups at different temperatures resulted in controlled post-functionalization of thermally reduced graphene oxide-triazine. Reaction conditions; i = *N*-methyl-2-pyrrolidon, 0 °C, 1 h and ii = sonication, stirring, room temperature 70 °C, 24 h. Reproduced with permission from ref. 35. Copyright 2017 WILEY-VCH Verlag GmbH & Co. KGaA, Weinheim.

GO layers with only hydroxyl groups have shown a small affinity towards VSV in comparison with the GO with a high density of sulphates. In physiological conditions, the sulphate groups are considered the main cause of the interaction between GO and viruses under physiological conditions. The virions do not show any change after binding to the sulphonated GO platform. The authors have, therefore, excluded any disinfection activity on VSV from the action of the reactive oxygens generated by GO.[16] A GO-based 2D platform composed of 6% graphene and 94% sulphated polyglycerol has been found to be able to trap 20 virions.

A very similar strategy has been developed by Ziem *et al.*,[32] to create a mimetic extracellular matrix *via* functionalization of graphene sheets with polyglycerol sulphates. The entry inhibition has been evaluated using two enveloped viruses with a double stranded DNA genome, *Pseudorabies Virus* (PrV, Suid herpesvirus 1) and *African swine fever virus* (ASFV). ASFV is an enveloped icosahedral, double stranded DNA virus of large dimensions (170–190 nm diameter). ASFV causes *African swine disease*, which is deadly for pigs.

The surface has been functionalized using linear or dendritic polyglycerol sulphate, which gives negatively charged GO platforms (Fig. 6). The linear polyglycerol azides have a higher inhibitory effect in comparison to the dendritic one in the case of PrV, but the effect is analogous for ASFV. The linear conformation favours the interaction with the virus

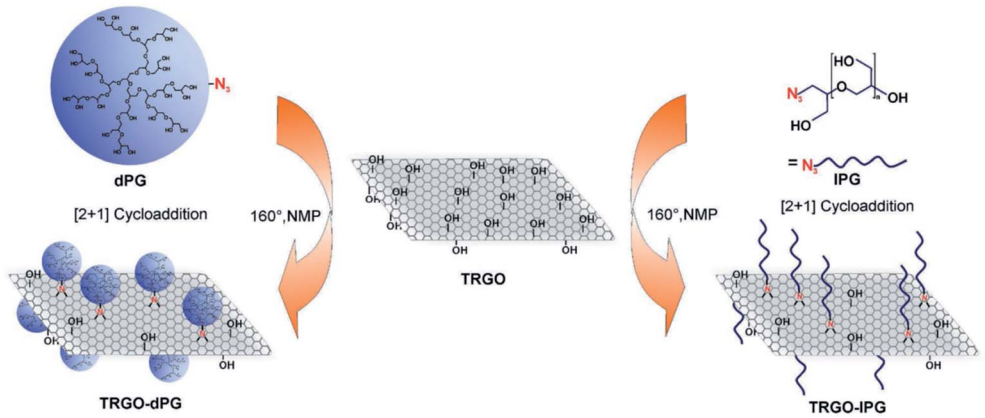

Fig. 6 Schematic representation of inhibitor development by combining thermally reduced graphene oxide (TRGO) with either dendritic polyglycerol (dPG) azide or linear polyglycerol (lPG) azide. Reproduced with permission from ref. 32. Copyright 2017 WILEY-VCH Verlag GmbH & Co. KGaA, Weinheim.

because it is more like the heparan sulphate in the extracellular matrix, which interacts with the herpes viral glycoproteins gB and gC.

Another graphene platform to bind viruses has been developed by Donskyi *et al.* who functionalized GO with polyglycerol sulphate and fatty amine functionalities.[34] The interaction of this platform with *Herpes Simplex Virus type 1* (HSV-1) has been studied. The combination of sulphate and alkyl chains produces binding of the virus through electrostatic interactions with the polyglycerol sulphate, while the alkyls induce a high antiviral activity through secondary hydrophobic interactions. Alkyl chains of different lengths (C_3–C_{18}) have been tested. Longer alkyl chains have been found to have the highest antiviral activity, but they are also toxic against Vero cells. The best compromise in terms of toxicity and antiviral effects is observed in layers functionalized with C_6 and C_9 alkyl chains.

GO has also been used as a platform for curcumin, a natural polyphenol, which is known for its antioxidant, antibacterial and antiviral activity.[33] Curcumin was efficiently linked to the GO surface *via* β-cyclodextrin molecules used as intermediate sites (Fig. 7). The antiviral effect of the system was tested with *Respiratory Syncytial Viruses* (RSV). RSV is an enveloped RNA virus (120–200 nm in diameter), belonging to the *Pneumoviridae* family and *Human Orthopneumovirus* species.

The antiviral activity of the nanosystem was explained on the basis of three different mechanisms that could synergistically operate: inhibition of the virus attachment on the surface of the cells, interference of virus replication and direct inactivation of the virus.

Controlling the graphene–virus interactions, which could be direct or mediated through surface functionalization, depends on several parameters. In particular, the dimensions, the number of layers, the surface wrinkling and the geometrical topology of the layers have a key role. The interaction of graphene with three key target proteins, HIV-Vpr, Nef and Gag, of HIV has been modelled to evaluate the effect of the number and size of layers.[36] The bonding affinity of graphene does not increase with the number of layers, and from 1 to 5 layers no changes should be expected on the basis of theoretical calculations. On the other hand, increasing the size produces an enhancement of the binding affinity.

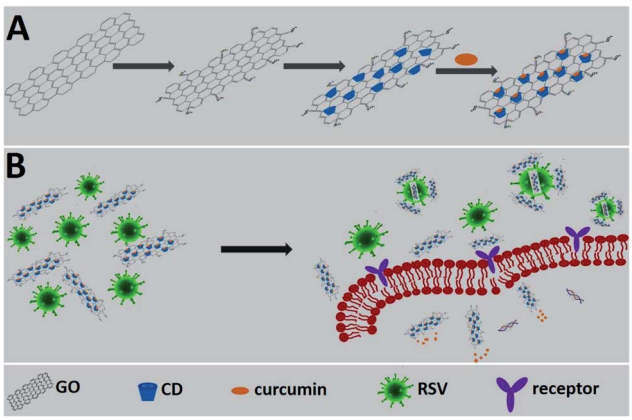

Fig. 7 Schematic representation of the working principle. (A) The synthesis of a functional nanomaterial composite. (B) The proposed inhibition mode of the functional nanomaterial composite against RSV infection. Reproduced with permission from ref. 33. Copyright 2017 The Royal Society of Chemistry.

2.5 Platform for antiviral drugs

The possibility of using GO as a platform has been, as we have seen, exploited to produce nanosystems with the capability of binding viruses, producing an extracellular matrix which blocks the virus before they can attach to the surface of the cell. Another possibility is using GO as a 2D platform to load drugs with a recognized antiviral activity. Hypericin (HY) is an anthrone derivative, which is widely used as an antiviral for several retrovirus, such as HSV-1, Sendai virus and duck hepatitis B. HY has been loaded on GO *via* physisorption, through π–π stacking and hydrophobic interactions.[37] The advantage of this approach is that HY is slowly released and this decreases its cytotoxic effect. The GO-HY system has shown an effective capability to inhibit viral replication using novel duck retrovirus as a model.

2.6 Search and destroy strategy

Functionalization of the graphene oxide surface with sulphonate groups allows binding of the viruses, avoiding or limiting the interactions with cells.[38] This strategy has been improved by anchoring on the graphene surface (Fig. 8). After the viruses have been captured by the graphene layers, they can be removed using magnetic nanoparticles and finally inactivated by exposure to near infrared radiation.

The high thermal conductivity of graphene is correlated to its excellent capability of light-to-heat conversion. This property has been used for photothermal[39] and photodynamic[40] treatments of cancer cells and bacteria. The sulphonated reduced graphene oxide with grafted magnetic iron nanoparticles has shown a remarkable capability to inactivate HSV-1. 99.99% of the virus was inactivated within 10 minutes upon irradiation with NIR light.

3. Antiviral effects of carbon dots

So far, we have seen that 2D materials, in this case graphene and graphene oxide, exhibit interesting antibacterial and antiviral properties and have relevant characteristics as functionalized platforms against viruses of various kinds. It is worth considering another family of carbon-based nanomaterials that has attracted great attention in recent years due to their excellent optical properties and ease of synthesis, the carbon dots (C-dots).[41–43]

Studies on the antiviral properties of carbon dots are very recent and in small numbers. Nevertheless, they show promising opportunities for such nanomaterials.

Carbonization of organic precursors can give carbon-based nanoparticles, whose structural characteristics, although still debated, can be easily engineered thanks to an appropriate

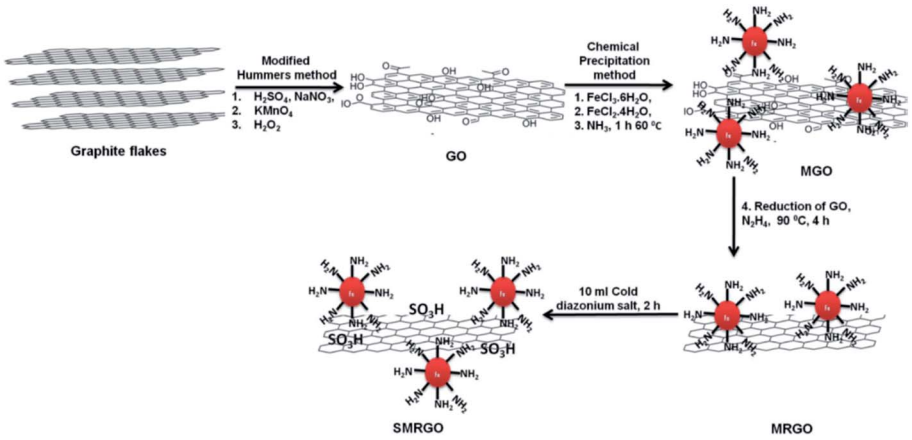

Fig. 8 First, graphite was oxidized to GO by a modification of Hummers' method. Next, the GO was functionalized with magnetic nanoparticles and reduced to MRGO. Finally, the MRGO was sulfonated to yield SMRGO. Reproduced with permission of ref. 38. Copyright 2017 American Chemical Society.

choice of precursors.[44–46] More precisely, C-dots represent a large family of carbon-based materials, whose structure is still under debate. Different types of nanomaterials are included in the family of C-dots, amorphous carbon nanoparticles, partially graphitized core–shell carbon nanoparticles, amorphous fluorescent polymeric nanoparticles and graphene quantum dots (GQDs). GQDs are small fragments of graphene, with a lateral size <10 nm, and share many properties with carbon dots and graphene. The large variety of C-dots results in potential applications ranging from photocatalysis to bioimaging. However, in addition to the remarkable optical properties that make them the main candidates for new generations of optoelectronic devices, C-dots have also shown an active role against infections. This is mainly due to the functional groups on their surface, which in turn are responsible for their extraordinary optical properties. As we will see, these functional groups influence the antiviral properties of C-dots, making them active against a virus or even determining their broad-spectrum effects.

Recent experiments have shown that some nanostructures functionalized with boronic acid are able to inhibit the entry of some viruses and block their attachment.[47] In the light of these results, C-dots made from boronic acid precursors have been recently particularly relevant. C-dots have been tested against *Herpes simplex Virus Type 1* (HSV-1) with encouraging results. The experiments were performed under classical *in vitro* conditions on monkey kidney cancer cells (Vero) and human lung cancer cells (A549), and cytotoxicity and antiviral assays were performed. The properties and functionality of three different types of C-dots, made with the hydrothermal technique, have been investigated. The precursors of C-dots have guaranteed the formation of different functional groups, revealed through vibrational spectroscopy techniques. Phenylboronic acid (PBA), 3-aminophenylboronic acid (3-APBA), or 4-aminophenylboronic acid hydrochloride (4-APBA) have been used as precursors. After treatment at 160 °C for 8 h the products were dialyzed before being used for *in vitro* studies.

The cytotoxicity study revealed that all three C-dots were non-cytotoxic towards A549 cells at concentrations of up to 300 μg mL^{-1}. Moreover, PBA and 4-APBA derived C-dots showed no cytotoxicity to Vero cells, although 3-APBA based C-dots were moderately cytotoxic. As shown in Fig. 9, at a concentration higher than 5 μg mL^{-1} of 3-APBA/C-dots and 4-APBA/C-dots, no infection was detected with 100% cell viability. On the contrary, PBA/C-dots have shown no effectiveness against virus infection. Interestingly, the role of C-dots can be revealed by a morphological study of the cells. As a result of virus presence, the cells undergo an important change in shape and dimensions, while being unaltered under

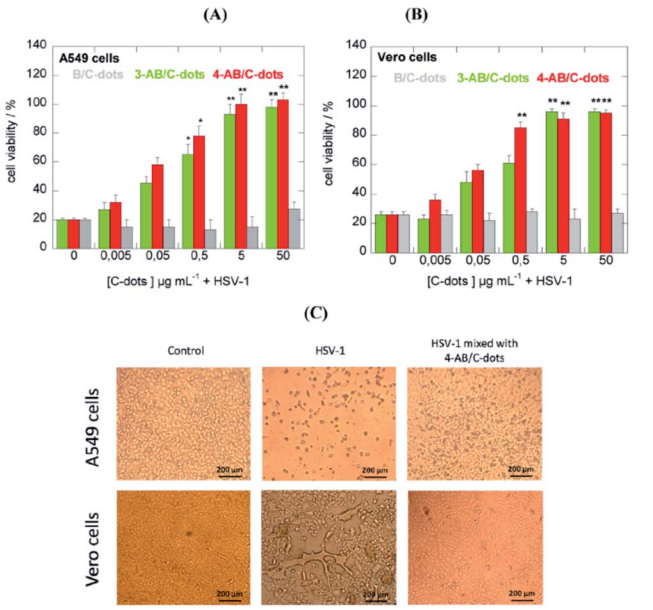

Fig. 9 C-dot inhibition effects of HSV-1 on A549 (A) and Vero (B) cells at different concentrations. (C) Morphological effects of C-dot treatments. Reproduced with permission from ref. 48. Copyright 2016 American Chemical Society.

treatment with C-dots. The contrasting mechanism of C-dots to the virus is not completely understood. Indeed, it has been confirmed that boronic acid is not involved in the inhibition of HSV-1, in contrast to other boronic acid-modified nanostructures. C-dots have a significant impact at the early stage of virus entry by interacting more with Vero cells than with viral entities, interfering with the interaction between cell receptors and the virus.[48]

The effect of virus inhibition of C-dots has also been tested with *Human Immunodeficiency Virus HIV-1* infections. HIV-1 is a *Retrovirida* family virus, with a diameter of 120–200 nm, which is responsible for the disease.

C-dots with a hydrodynamic diameter of about 3 nm have been prepared by carbonization of anhydrous citric acid at 200 °C for 30 min and dialyzed thereafter. The obtained C-dots have also been functionalized with 4-carboxy-3-chlorobenzeneboronic acid (CBBA/C-dots). In this case, the role of boronic acid groups has been pointed out. C-dots and CBBA/C-dots have been mixed with MOLT-4 cells to assess the cytotoxicity. Both dots appeared safe, up to a high concentration of 300 μg mL^{-1}, with cell viability over 80% even at 300 μg mL^{-1}. The corresponding CC_{50} values were 2901.2 and 1991.9 μg mL^{-1}. The antiviral role of C-dots and CBBA/C-dots has been studied by evaluating syncytia formation. Indeed, one of the most efficient routes of virus transition from an infected cell to a normal cell takes place with direct contact. Counting the numbers of syncytia in the presence of dots can be a good way of evaluating the virus infection. As a result, C-dots have not prevented the formation of syncytia, while CBBA/C-dots have bonded to gp120 on the virus, blocking the infection by preventing the MOLT-4 cells from binding (Fig. 10). Although hydroxyl and carboxylate surface groups on C-dots can inhibit HIV infection by the formation of hydrogen bonding with the molecules of the viral envelope, the boronic acid tends to enhance this effect, by interacting with 1,2-*cis* diol sites on gp120.[49]

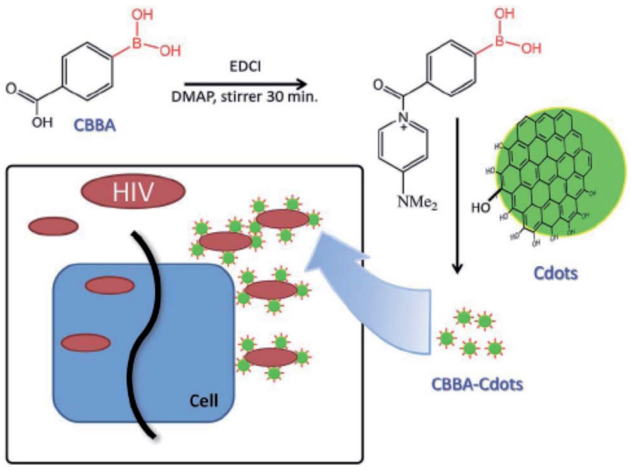

Fig. 10 Proposed mechanism *via* which CBBA/C-dots inhibit the entry of HIV-1. Reproduced with permission from ref. 49. Copyright 2016 The Royal Society of Chemistry.

PEG-diamine and ascorbic acid derivate C-dots have shown encouraging results as viral inhibitors by active functionality. The dots, showing a low level of cytotoxicity with cell viability of 72% after 48 h incubation at the concentration of 0.250 mg mL^{-1}, have been tested on Monkey kidney (MARC-145) and Porcine kidney (PK-15) cells. In particular, MARC-145 cells have been infected by porcine reproductive and respiratory syndrome virus (PRRSV) and PK-15 by *Pseudorabies Virus* (PRV). The virus titers were reduced in the presence of C-dots in comparison with the control groups (Fig. 11). PRV has also been studied by indirect immunofluorescence assay of PRV-gD and PRV-VP16, which is responsible for binding with host cell receptors and is a component of primary enveloped virions, respectively. The samples treated with C-dots showed a significant decrease in fluorescence in accordance with the titer count. The experiments on PRRSV gave the same conclusions, with remarkable inhibitory effects of CDs. At the same time, the investigation of type I interferons (IFNs) α, antiviral innate immune molecules, and the IFN-stimulated genes (IFGs) has indicated a possible inhibitory mechanism of C-dots *via* the activation of IFN-α and production of ISGs.[50]

Similar results have been obtained for curcumin derived C-dots, exploiting the antiviral activity of herbs.[51,52] They have been applied to porcine epidemic diarrhoea virus (PEDV) as a coronavirus model. Ting *et al.* have treated a mixture of citric acid and curcumin at 180 °C for 1 h under hydrothermal conditions (CCM/C-dots) and compared the resulting C-dots with the more common ethylenediamine-based dots (EDA/C-dots). It was found that CCM/C-dots display a great efficacy against the replication of PEDV in comparison with EDA/C-dots. In fact, CCM/C-dots can modify the structure of the surface proteins in viruses, suppress the negative-strand RNA of the virus and the accumulation of reactive oxygen species, and stimulate the production of ISGs and cytokines. The inhibition of PEDV in Vero cells at the CCM/C-dot concentration of 125 μg mL^{-1} was studied by monitoring the titer counts and green fluorescence signal of PEDV N proteins. The CCM/C-dots present a positive charge, and so strongly interact with PEDV and the cell membrane, competing with the virus to bind to the cell surface. The z-potentials of CCM-CDs, PEDV and CCM-CDs pre-treated with PEDV were +15.6, −6.42 and −0.18 mV, respectively. Therefore, the positive potential of the C-dots can promote the aggregation of the virus and reduce the infectivity, as verified by fluorescence and Raman measurements.[52]

Although the mechanism of action of carbon dots is still far from being fully understood, it has been well established that the role of functional groups deriving from the appropriate choice of different precursors is a fundamental parameter. This is what emerged from the experiments of Łoczechin *et al.*,[53] where different C-dots were tested as a countermeasure to the proliferation of *HCoV-229E Human Coronavirus* in Huh-7 cells. HCoV-229E is an enveloped, single-stranded RNA coronavirus. It is one of the viruses that cause the common cold with a 120–160 nm diameter (*Coronaviridae* family, *Human coronavirus 229E* species). As in previous works, the primary role of C-dots is to act at the early stages of infection, inhibiting the interaction of the S-receptor protein with the host cell

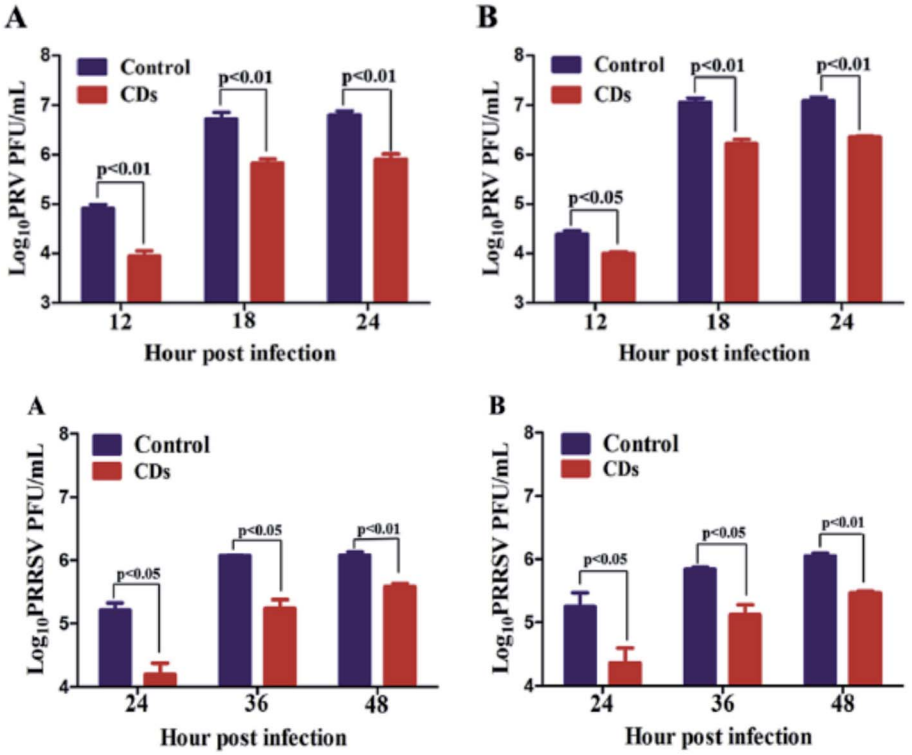

Fig. 11 The replication process of PRV (top) and PRRSV (bottom). Reproduced with permission from ref. 50. Copyright 2016 Elsevier Ltd.

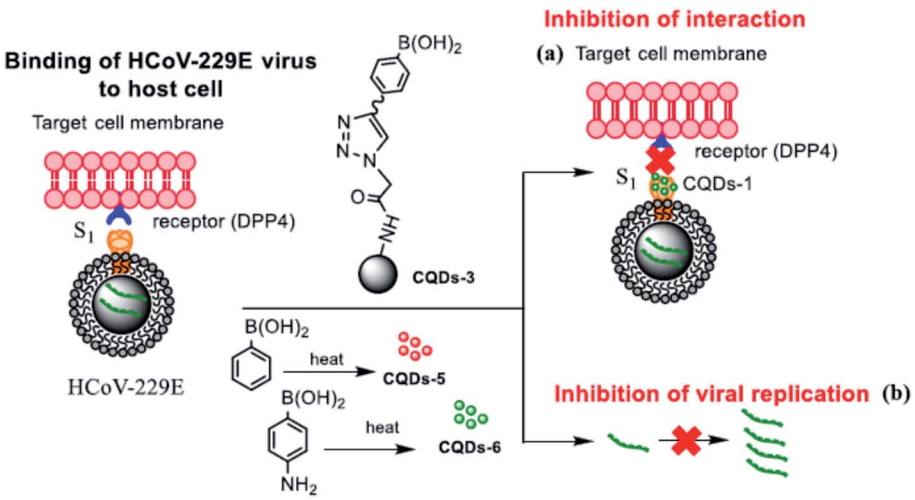

Fig. 12 Scheme of the carbon dot inhibition mechanism of HCoV-229E. Reproduced with permission from ref. 53. Copyright 2019 American Chemical Society.

membrane (Fig. 12). However, not all C-dots have shown the same effectiveness, underlining the importance of molecular groups resulting from synthesis. In this work, the first group of C-dots was synthesized by hydrothermal carbonization of ethylenediamine/citric acid and functionalized according to the scheme in Fig. 13.

In general, the highest efficacy of C-dots occurs in the first period after infection, at about 1 h after inoculation. However, they showed significant inhibition activity even after 5.5 h. Still, the mechanism of inhibition must be figured out, although it seems to be based on the interaction with cells.

Lin *et al.*[51] have suggested that C-dots can act at different levels of infection. Again, curcumin derived C-dots were realized by pyrolyzing curcumin at different temperatures. The C-dots were then tested against EV71 virus in RD cells. C-dots can hinder the interaction of the virus with RD cell membranes. In addition, they can suppress the ROS (reactive oxygen species) by working as radical scavengers and inhibit PGE_2 production.

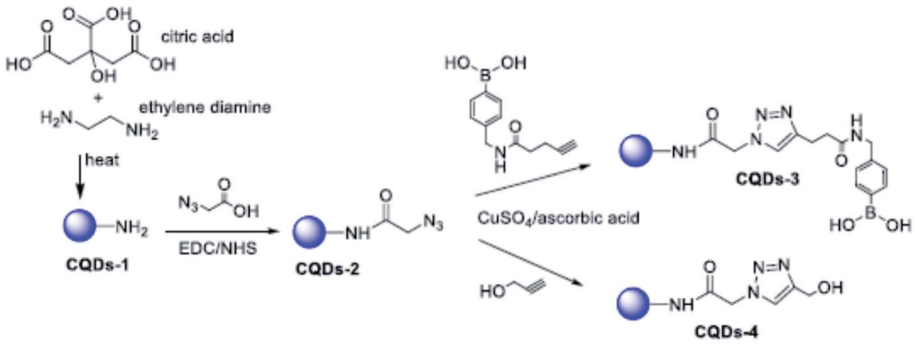

Fig. 13 Scheme of the functionalization of EDA/citric acid derived C-dots. Reprinted with permission from ref. 53. Copyright 2019 American Chemical Society.

Furthermore, it has also been reported that curcumin C-dots can decrease the expression of p38 kinase.[50]

A further step forward is represented by C-dots from benzoxazine. Contrary to the previous examples, where an important role of boronic acid was highlighted, in this case the effectiveness of boron-free C-dots has been demonstrated. In addition to the well-known biocompatibility, these hydrothermally synthesised C-dots made from the monomer benzoaxine BZM have demonstrated broad spectrum efficacy in blocking virus infectivity. Unlike other systems, where multiple mechanisms can intervene in antiviral activity, in this case the C-dots have shown a direct interaction with virions. C-dots have been employed against flaviviral (JEV) infections in BHK-21 cells.[54] To investigate the broad-spectrum potential of C-dots, different viruses have been treated, both enveloped and non-enveloped. Although the dots present a marked effect on JEV and ZIKV, they have been demonstrated to be suitable for other viruses. The EC_{50} of BZM/C-dots against different viruses is 18.63 μg mL^{-1} (JEV), 3.715 μg mL^{-1} (ZIKV), 37.49 μg mL^{-1} (DENV), 40.25 μg mL^{-1} (AAV), and 45.51 μg mL^{-1} (PPV).[54]

Finally, it is worth mentioning that carbon nanoparticles with 2,2′-(ethylenedioxy)bis(ethylamine) and 3-ethoxypropylamine have been proved to inhibit the interaction of human norovirus virus-like-particles (VLPs) with HBGA receptors, leaving intact the morphology of the VLP particles.[55] Additionally, VLPs have been hampered in interacting with their respective antibodies.

Unlike the other carbon materials within the C-dot classification, whose optical properties are mainly governed by the presence of fluorophores or functional groups produced during the synthesis, the photoluminescence of GQDs originates from quantum confinement effects, related to their size. Thus, the fluorescence emission can be tuned through changing the size of the graphene monolayers. GQDs can be obtained by thermal oxidation of graphene oxide, where epoxy and hydroxyl groups operate as cleavage sites and promote the cutting of GO into smaller fragments.[56,57] Mixtures of acids, *e.g.* nitric and sulphuric, are often employed for oxidative cleavage of graphitized carbon-based materials, although there are non-acidic alternatives such as oxone and H_2O_2. In addition, the electrochemical cutting of graphene, graphite, coal and so on, and ultrasonic exfoliation, allow for high yield GQD production.[58,59] GQDs have attracted a lot of attention because of their extraordinary potential in the biomedical field. In particular, they have been proven to be efficient and biocompatible emitters,[60] which can be used for the detection of *Hepatitis C Virus* core antigen[61] and *hepatitis B virus*,[62] and cancer-targeted fluorescent imaging.[63] GQDs have shown remarkable antiviral activity against HIV-1 infections. The most important experimental evidence of this efficacy has been reported by Iannazzo *et al.*[64] and it remains the most significant so far. In their work, GQDs were synthesized by acid oxidation and exfoliation of multiwalled carbon nanotubes. The activity of pristine dots has been compared with the antiretroviral agents CHI499 and CDF119. Furthermore, GQDs have been conjugated with CHI499 and CDF119 as drug delivery systems. The systems were tested as inhibitors of HIV in cellular and enzyme assays, whilst the cytotoxicity was studied in MT-4 cells. GQDs have shown antiviral activity with an IC_{50} of 37.6 μg mL^{-1}, and an EC_{50} value in cells of 19.9 μg mL^{-1}. Among the different candidates, the GQD/CHI499 system displays the most encouraging results. Indeed, the conjugated platform showed improved antiviral properties, with an IC_{50} of 0.09 μg mL^{-1} and an EC_{50} of 0.066 μg mL^{-1} and a selectivity index of 362. Accordingly, it has been supposed that the efficacy as drug delivery relies on the imide bond in GQD/CHI499. After drug release in the infected cells, both GQD and CHI499 can synergistically act as inhibitors. On the contrary, the amide bond in GQD/CDF119 prevents easy drug release.[64] Although the results open new opportunities for antiviral applications, GQDs have displayed more significant potential in bioimaging and sensing.[58,65]

4. Fullerenes as antivirals

Fullerene and its derivatives were the first class of carbon-based nanostructures to be discovered (1985) and their chemistry and properties have been the subject of extensive investigations. Potential biological applications in several fields have been developed using specific fullerene derivatives.[66] Fullerenes were also the first carbon compound to be tested, in comparison to graphene and C-dots, as an antiviral.

4.1 Fullerenes as anti-HIV agents

The first report on the antiviral activity of fullerenes dates back to 1993.[67] It was recognized that fullerene derivatives have an anti-HIV activity by blocking its encoded enzymes because the bulky fullerenes fit well into the active sites of HIV protease. A diamido diacid diphenyl fulleroid derivative was specifically designed to inhibit an HIV enzyme. Since then several research groups have worked on tailoring the synthesis of fullerene derivatives to inhibit the activity of HIV enzymes, HIV-1 RT and DNA polymerase. The general strategy is the same, developing a fullerene derivative able to inhibit the HIV enzymes. Different antiviral effects have been observed depending on the fullerene functionalization.[68–77] A comparative table with the main results can be found in ref. 78. The main problem is balancing the cytotoxicity with the antiviral activity. In general, low cytotoxic effects have been observed for fullerene derivatives but the data still need more experiments to fully address some critical points, such as the presence and the effects of C_{60} derivative isomers.

The low solubility of fullerenes in water represents a strong limitation for their applications in biology.[79] The preparation of soluble derivatives is, therefore, a mandatory step. An example of antiviral application of highly water-soluble fullerene derivatives was reported by Troshima *et al.* in 2007.[80] Using chlorofullerene, $C_{60}Cl_6$, as a precursor substrate, polycarboxylic fullerenes in high yield were obtained. The fullerene derivatives in the form of alkali metal salts have a high solubility in water (50–100 mg mL^{-1} at pH < 7.5) and a significant anti-HIV activity with a low cytotoxicity. Another question to be addressed is the potential antiviral activity of water soluble derivatives of fullerenes with larger carbon cages, such C_{70}. In comparison to C_{60}, because of the lower symmetry, the synthesis of C_{70} water soluble derivatives is more difficult. Kornev *et al.* prepared highly soluble C_{70} compounds whose antiviral activity and cytotoxicity were tested.[81] A significant antiviral activity against HIV and influenza virus, H1N1 and H3N3, was detected. *Influenza A virus* subtype H1N1 is a subtype of *Influenza A* virus, belonging to the *Orthomyxoviridae* family (80–120 nm in diameter). H3N3 is another type of *Avian influenza virus* of the same family. Interestingly, a new antiviral mechanism, through the interaction of the C_{70} derivatives with the envelope gp120 protein from HIV-1(III_B), has been observed. This protein is used by the virus to enter the cells *via* specific surface receptor recognition.

Besides HIV, the inhibition of viral activity by fullerene derivatives has been tested for *hepatitis C virus* (HCV),[82] *respiratory syncytial virus* (RSV),[83] *virus H1N1*, *herpes simplex virus*,[84] *human cytomegalovirus*,[84] *Zika* and *Dengue viruses*.[85]

4.2 Antiviral activity of non-derivatized fullerenes

An interesting question arises: is pristine C_{60} capable of any direct effect on viruses? Non-derivatized C_{60} has been found to inhibit the replication of simian immunodeficiency virus (SIV) and the activity of *Moloney Murine Leukemia virus* (M-MuLV) reverse transcriptase.[77] The 50% inhibitory concentration (EC_{50}) of non-derivatized C_{60} was 3 μM, but an explanation of the mechanism has not been reported.

4.3 Viral inactivation *via* photosensitized production of singlet oxygen by C_{60}

An important property of fullerene is the capability of generating singlet oxygen ($^1O_2$) with a high quantum yield, 0.96, upon

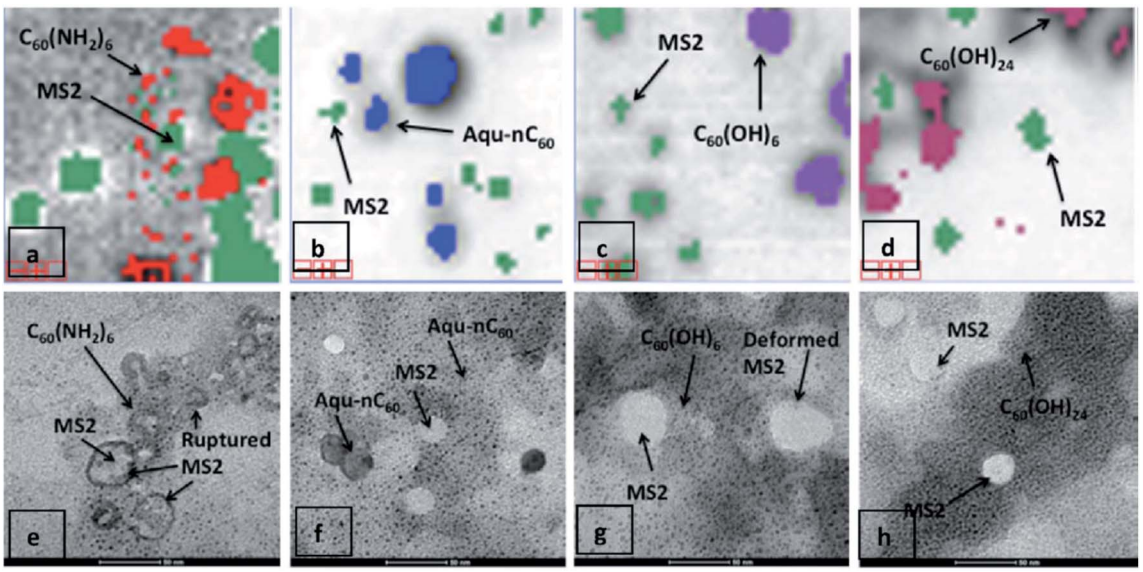

Fig. 14 Relative proximity of various fullerenes with MS2 following mixture-tuned matched filtering analysis of hyperspectral images. 5-Fold zoomed-in views (1 cm = 20 μm) of noise-free image data with superimposed classification results are shown. MS2 viruses appear as green pixels after staining with 2.5% phosphotungstic acid. $C_{60}(NH_2)_6$ is shown as red colour (a), aqu-nC_{60} as blue (b), $C_{60}(OH)_6$ as purple (c), and $C_{60}(OH)_{24}$ as pink (d). Corresponding TEM images after sample dehydration are shown in (e–h). Reproduced with permission from ref. 96. Copyright 2012 American Chemical Society.

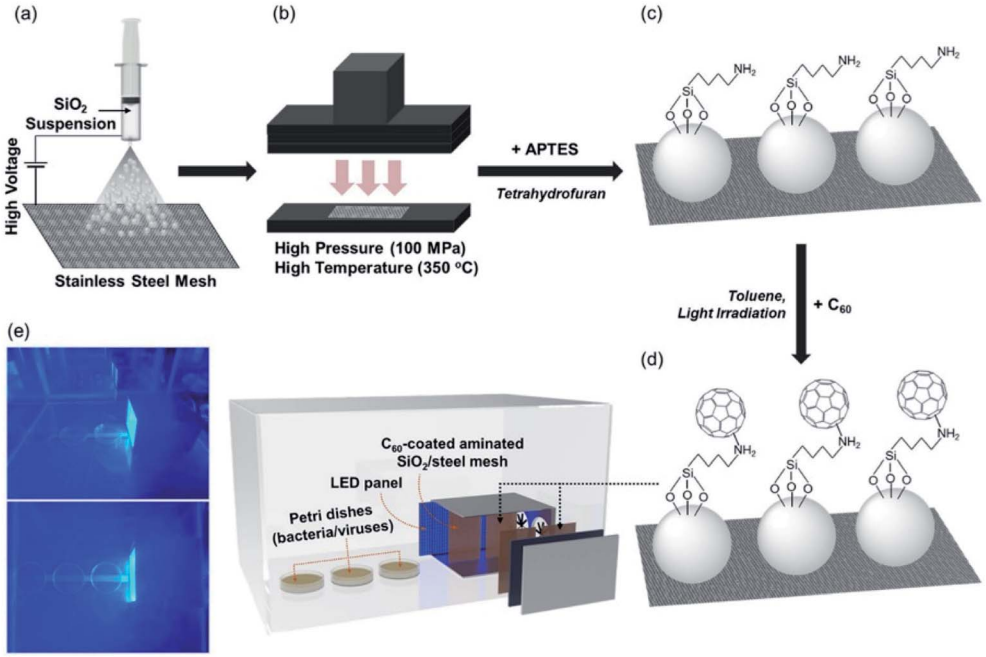

Fig. 15 (a) Electrospraying silica particles (dispersed in methanol) on stainless-steel mesh; (b) hot pressing; (c) amination of silica loaded on stainless-steel mesh with 3-aminopropyltriethoxysilane; (d) covalent C_{60} attachment through nucleophilic addition of primary amines; and (e) use of C60 immobilized on the amine-functionalized silica-coated stainless steel mesh for visible-light-sensitized remote singlet oxygenation. Reproduced with permission from ref. 100. Copyright 2020 Elsevier Ltd.

illumination in the visible region (535 nm).[86] The generation of singlet oxygen[87,88] by fullerenes has been used for antimicrobial[89] applications and for the removal of pollutants.[90] Singlet oxygen as an oxidant in comparison to hydroxyl radicals (˙OH) is characterized by a longer lifetime (τ), 2–4 μs with respect to 1 ns for ˙OH. Hydroxyl radicals are also non-selective oxidants while singlet oxygen, which has a low reduction potential, is more specific. Several research groups have explored the possibilities of using photoactivated fullerene and some of its derivatives as antiviral agents.

A first set of experiments was dedicated to investigating the photodynamic inactivation of enveloped viruses by suspensions of non-derivatized C_{60}. Based on the known effect of singlet oxygen on virus inactivation,[91] C_{60} suspensions were used as inactivating agents. The low solubility of fullerenes, in this case, is a positive property because it allows, in principle, easier and complete removal of the photosensitizer from aqueous solutions.[92–94] Other sensitizers, such as hypericin, that remain in biological fluids can be potentially toxic. An aqueous fullerene suspension has been used as a photosensitizer to inactivate an enveloped virus, H1N1, in the allantoic fluid of chicken embryos.[95] Damage of the surface membrane and loss of surface glycoproteins was observed upon irradiation for at least 2 hours.

Four different photosensitized aqueous fullerene suspensions have been used to inactivate the *MS2 bacteriophage*.[96] The ($^1O_2$) generation rate follows the order: $C_{60}(NH_2)_6 > C_{60}(OH)_{24} \approx$ aqu-$nC_{60} > C_{60}(OH)_6$. The singlet oxygen produces an alteration of the capsid protein secondary structures and protein oxidation. MS2 inactivation appears to be the result of the loss of capsid structural integrity and the reduced ability to eject genomic RNA into its bacterial host has been considered the cause of MS2 inactivation (Fig. 14).

The main application of fullerene suspensions that has been envisaged is to prevent the transmission of viral infections *via* plasma.[97] Using C_{60} as a photosensitizer has been shown to allow full inactivation of enveloped viruses in irradiated plasma.

Inactivation of *MS2 bacteriophage* has also been demonstrated in the case of fullerene derivatives. Cationic amine-functionalized C_{60} derivatives,[98] tris-adducted fulleropyrrolidinium aggregates,[99] have shown a remarkable antiviral activity even if a direct comparison in terms of inactivation capability is difficult because of the different experimental conditions. A dependence of the inactivation efficacy on the intensity of light and concentration of fullerenes has been observed.[84]

Another possibility is using fullerenes to create a photoactive platform capable of remote inactivation of viruses and bacteria. A substrate of hot-pressed silica particles deposited on a metallic substrate was functionalized with 3-aminopropyltrietoxysilane and the amine groups used to covalently attach the fullerenes.[100] The inactivation of the *MS2 bacteriophage virus* was studied at predefined distances from the irradiated surface. Inactivation of the virus *via* singlet oxygen was observed to be effective up to around 10–15 cm from the surface (Fig. 15).

Another important property to consider in developing an antiviral platform based on UV irradiation of fullerenes is their radical sinking effect.[101] This reduces the efficiency of binary systems formed by titania, which upon UV irradiation generates free radicals, and fullerenes, which act as radical sinks.

Table 1 Summary of carbon-based nanomaterials as antivirals

Virus	Family	Species	Nucleic acid	Viral envelope	Carbon-based materials	Ref.
PEDV	Coronaviridae	*Porcine epidemic diarrhoea virus*	RNA	Enveloped	GO, C-dots	18 and 52
FCoV		*Alphacoronavirus 1*			GO-AgNPs	30
HCoV-229E		*Human coronavirus 229E*			C-dots	53
SuHV-1 (PRV)	Herpesviridae	*Suid alphaherpesvirus 1*	DNA	Enveloped	GO, C-dots	18 and 50
HSV-1		*Human alphaherpesvirus 1*			GO, C-dots, GQDs, fullerene	20, 27, 32, 34, 38, 48, 49, 64 and 84
HCMV		*Human betaherpesvirus 5*			Fullerene	84
H9N2	Orthomyxoviridae	*Influenza A*	RNA	Enveloped	GO	21
H1N1					Fullerene	81, 91, 95 and 97
H3N2					—	—
H3N3					Fullerene	81
EV71	Picornaviridae	*Enterovirus A*	RNA	Non-enveloped	GO, C-dots	21 and 51
MS2 bacteriophage	Leviviridae	*Escherichia virus*	RNA	Non-enveloped	GO, fullerene	24–26, 96, 98 and 99
IBDV	Birnaviridae	*Infectious bursal disease virus*	RNA	Non-enveloped	GO-AgNPs	30
PRRSV	Arteriviridae	*Betaarterivirus suid 1*	RNA	Enveloped	GO-AgNPs, C-dots	31 and 50
VSV	Rhabdoviridae	*Indiana vesicolorum*	RNA	Enveloped	GO	35
ASFV	Asfarviridae	*African swine fever virus*			TRGO-PG	32
HIV	Retroviridae		RNA	Enveloped	G, fullerene	36 and 81
SIV					Fullerene	77
M-MuLV		*Murine leukemia virus*			Fullerene	77
NDRV	Reoviridae		RNA	Non-enveloped	GO/HY	37
JEV	Flaviviridae	*Japanese Encephalitis virus*	RNA	Enveloped	C-dots	54
ZIKV		*Zika virus*			C-dots, fullerene	52 and 85
DENV		*Dengue virus*				54 and 85
HCV		*Hepacivirus C*			Fullerene	82
AAV	Parvoviridae	*Adeno-associated dependoparvovirus*	DNA	Non-enveloped	C-dots	54
PPD		*Ungulate protoparvovirus 1*			C-dots	54
RSV	Pneumoviridae	*Human orthopneumovirus*	RNA	Enveloped	GO, fullerene	33 and 83

5. Summary and future outlook

The request for antiviral solutions has recently drawn the attention of the scientific community towards innovative solutions. Nanomaterials, because the scale and surface properties can be specifically engineered, are potentially disruptive new antiviral tools.

Many of these materials are already leading players in nanotechnology, with a key role in several research fields, such as photocatalysis, photonics and optoelectronics. Metallic and oxide nanoparticles, in particular, have been widely tested as antiviral materials,[102] but several questions remain to be solved, such as the cytotoxicity, which still needs to be fully assessed. This is the reason why we have not included in the present review another important class of carbon-based nanomaterials, the carbon nanotubes. Their potential toxicity still represents, in fact, a major issue. Carbon-based nanomaterials are, however, interesting candidates for antiviral applications, in particular graphene, carbon dots and fullerenes.

Table 1 shows a summary of the main carbon nanomaterials that have been tested as antivirals. The large variety of combinations suggest that the studies in this field are still in the exploratory phase and much work needs to be done. In particular, an important general question which has to be studied and assessed is the relationship between the C-dot dimensions and shape and that of the virus. The possibility of fabricating C-dots that simulate the virus shape and surface is a very challenging issue, but specific and systematic studies have to be carefully performed.

In addition to the carbon-based nanomaterials considered in this overview, it is worth mentioning the nanodiamonds (NDs), which, with their particular surfaces and dimensions, are potential candidates of importance in nanomedicine.[103] NDs are among the smallest carbon-based materials and are, conventionally, crystalline nanoparticles of about 5 nm in size.[104] Their unique characteristics derive from the physicochemical properties of the particle facets. NDs can be obtained by the detonation of explosive carbon-based materials. Some of the particles are crystalline carbon objects below 10 nm.[105] This procedure suffers from several drawbacks, including the high quantity of impurities, which requires purification work. Among the most common impurities are metals and carbon-based systems with a different structure from that of the diamond. Over the years, numerous purification processes have been implemented, including oxidative treatments in the liquid or gaseous phase and acid treatments.[103,106–109] One of the most severe drawbacks that can be encountered in the use of NDs is their tendency to aggregate, leading to the formation of clusters of hundreds of nanometres. This phenomenon is facilitated by the presence on the surface of functional groups (carboxylic, hydroxylic, *etc.*) capable of generating hydrogen or covalent bonds, determining high adhesion forces. NDs can be easily functionalized for specific biological applications. The surface functional groups determine the chemical environment of use and the interactions with tissues, and can improve the biocompatibility. Among post-synthesis processes, graphitization to obtain sp^2 carbon on the surface, hydrogeneration, silanization and reactions with amines or PEG[103] are the most common. To date, no studies have investigated the antiviral activity of NDs. However, considerable efforts have been made to study the toxicological properties and biocompatibility of NDs. In particular, it has been demonstrated that purified NDs do not show significant toxicity. Ivanova *et al.*[110] reported the effects of ND interaction with influenza viruses. This study highlighted the absorbency of NDs against viruses. Viruses such as *Influenza A* H1N1 and H3N2 were concentrated and placed in a solution of NDs. Hemagglutination tests with erythrocytes were used for virus detection. Absorption and desorption studies have highlighted the possibility of using NDs as antimicrobial filters. NDs have shown encouraging results in attaching to the envelopes of *E. coli* and as an antibacterial. The most promising results highlight that NDs have relevant properties as potential drug delivery systems, with numerous engineering and functionalization possibilities.[104] As an antiviral, the current literature does not show emerging opportunities and a greater effort has to be made to improve current knowledge about the cytotoxicity and purification of such systems.

Regarding the prospects of graphene as an antiviral material, we also have to distinguish between graphene and graphene oxide. Graphene oxide has antibacterial activity and, to a lesser extent, also antiviral properties, well documented for pseudorabies viruses. However, the characteristics of low toxicity and surface functionalization allow graphene to be thought of as a useful platform in combination with other antiviral systems acting on the nanoscale. For this reason, most of the experiments have used GO to exploit the possibilities of surface functionalization. GO and graphene have high potential for virus detection, but their direct use as an antiviral is also more difficult to forecast because their dimensions and shape are large on the nanoscale and difficult to control. However, to date, there are no systematic studies that allow clear identification of the antiviral mechanism to be achieved, and specific studies have to be performed to understand the graphene–virus interaction. It has been suggested that the virucidal activity is due to physical disruption of the virus by the sharp edges of graphene. It is not clear, however, if this mechanism works in general or only for specific types of virus.

Among the latest tested antiviral systems, carbon dots have shown encouraging results in terms of biocompatibility and antiviral properties. Carbon dots have many advantages. They can be easily synthesised from a few precursors through a process based on carbonisation. The surface of these nanomaterials can be properly engineered either in the synthesis phase through the choice of precursors or through a post-synthesis functionalization. The main problem with C-dots is the lack of a single model applicable to interaction with viruses. The variety of C-dot species is potentially endless and it is necessary to create a shortlist of a few potential candidates to be tested for cytotoxicity and antiviral activity studies. To date, the literature is rich in a multiplicity of papers focused on the synthesis of carbon-based particles, but lacking in systematic

investigations on the role of surfaces, size, shape and functional groups.

Despite the encouraging results, there is still much to be done for the use of carbon-based nanomaterials in nanomedicine. Although carbon dots have revealed significant antiviral activity, the success rate of most C-dots is remarkable in the early stages of the infection, when the nanoparticle seems to have a role in interfering with the interaction mechanism between the virion and cell. To date, one of the main obstacles to an improvement in antiviral properties against a specific virus is the lack of knowledge of the mechanism of action. In fact, as we have seen, the dependence of antiviral activity on some surface functional groups of the nanoparticles is contradictory and not fully demonstrated. Moreover, it is not clear whether C-dots are able to attack the virus directly, playing a virucidal role. Finally, there are many *in vitro* experiments, while *in vivo* ones are still scarce, and they are necessary to know the real potential of such systems. Another advantage of C-dots is the possibility of tailored surface functionalization, but on the other hand their structure is only defined in terms of properties and a specific control is still difficult to achieve.

Fullerenes have also shown remarkable properties as antiviral nanosystems. They have the advantage, with respect to graphene and C-dots, of having a well-defined composition and shape and a well-established functionalization chemistry. Fullerenes have also been widely studied as anti-HIV agents with promising results using different types of derivatives, but also in this case the cytotoxicity needs to be carefully evaluated. Fullerenes can generate a large amount of singlet oxygen which could be used to destroy the viruses and sanitize surfaces.

The exploration of antiviral properties and applications of carbon-based nanomaterials is still a new field and much research is still needed to assess the potential in this field. Carbon nanomaterials have, however, the potential to create antiviral systems with reduced toxicity. A full assessment of cytotoxicity appears to be the main issue to allow the development of antiviral applications for such classes of materials.

Conflicts of interest

There are no conflicts to declare.

References

1 V. Cagno, P. Andreozzi, M. D'Alicarnasso, P. J. Silva, M. Mueller, M. Galloux, R. Le Goffic, S. T. Jones, M. Vallino, J. Hodek, J. Weber, S. Sen, E. R. Janecek, A. Bekdemir, B. Sanavio, C. Martinelli, M. Donalisio, M. A. R. Welti, J. F. Eleouet, Y. Han, L. Kaiser, L. Vukovic, C. Tapparel, P. Král, S. Krol, D. Lembo and F. Stellacci, *Nat. Mater.*, 2018, **17**, 195–203.

2 P. P. Dechant, J. Wardman, T. Keef and R. Twarock, *Acta Crystallogr., Sect. A: Found. Adv.*, 2014, **70**, 162–167.

3 A. a. Hassan, M. K. Mansour, R. M. H. Sayed El Ahl, A. M. a. El Hamaky and N. H. Oraby, *Toxic and beneficial effects of carbon nanomaterials on human and animal health*, Elsevier Inc., 2020.

4 A. Pinna, L. Malfatti, G. Galleri, R. Manetti, S. Cossu, G. Rocchitta, R. Migheli, P. A. Serra and P. Innocenzi, *RSC Adv.*, 2015, **5**, 20432–20439.

5 A. Pinna, E. Cali, G. Kerherve, G. Galleri, M. Maggini, P. Innocenzi and L. Malfatti, *Nanoscale Adv.*, 2020, **2**, 2387–2396.

6 G. Chen, I. Roy, C. Yang and P. N. Prasad, *Chem. Rev.*, 2016, **116**, 2826–2885.

7 F. M. Tonelli, V. A. Goulart, K. N. Gomes, M. S. Ladeira, A. K. Santos, E. Lorençon, L. O. Ladeira and R. R. Resende, *Nanomedicine*, 2015, **10**, 2423–2450.

8 H. Roy, S. Bhanja, U. P. Panigrahy and V. K. Theendra, *Graphene-Based Nanovehicles for Drug Delivery*, Elsevier Inc., 2018.

9 D. De Melo-Diogo, R. Lima-Sousa, C. G. Alves and I. J. Correia, *Biomater. Sci.*, 2019, **7**, 3534–3551.

10 O. Akhavan, *Graphene scaffolds in progressive nanotechnology/stem cell-based tissue engineering of the nervous system*, 2016, vol. 4.

11 L. Shang, Y. Qi, H. Lu, H. Pei, Y. Li, L. Qu, Z. Wu and W. Zhang, *Graphene and graphene oxide for tissue engineering and regeneration*, Elsevier Inc., 2019.

12 D. Du, Y. Yang and Y. Lin, *MRS Bull.*, 2012, **37**, 1290–1296.

13 J. Lin, X. Chen and P. Huang, *Adv. Drug Deliv. Rev.*, 2016, **105**, 242–254.

14 W. Hu, C. Peng, W. Luo, M. Lv, X. Li, D. Li, Q. Huang and C. Fan, *ACS Nano*, 2010, **4**, 4317–4323.

15 S. Liu, T. H. Zeng, M. Hofmann, E. Burcombe, J. Wei, R. Jiang, J. Kong and Y. Chen, *ACS Nano*, 2011, **5**, 6971–6980.

16 O. Akhavan and E. Ghaderi, *ACS Nano*, 2010, **4**, 5731–5736.

17 C. Lee, *Virol. J.*, 2015, **12**, 193.

18 S. Ye, K. Shao, Z. Li, N. Guo, Y. Zuo, Q. Li, Z. Lu, L. Chen, Q. He and H. Han, *ACS Appl. Mater. Interfaces*, 2015, **7**, 21578–21579.

19 L. E. Pomeranz, A. E. Reynolds and C. J. Hengartner, *Microbiol. Mol. Biol. Rev.*, 2005, **69**, 462–500.

20 M. Sametband, I. Kalt, A. Gedanken and R. Sarid, *ACS Appl. Mater. Interfaces*, 2014, **6**, 1228–1235.

21 Z. Song, X. Wang, G. Zhu, Q. Nian, H. Zhou, D. Yang, C. Qin and R. Tang, *Small*, 2015, **11**, 1771–1776.

22 J. B. Gc, R. Pokhrel, N. Bhattarai, K. a. Johnson, B. S. Gerstman, R. V. Stahelin and P. P. Chapagain, *Biochem. Biophys. Res. Commun.*, 2017, **493**, 176–181.

23 K. Krishnamoorthy, R. Mohan and S. J. Kim, *Appl. Phys. Lett.*, 2011, **24**, 2013–2016.

24 X. Hu, L. Mu, J. Wen and Q. Zhou, *Carbon*, 2012, **50**, 2772–2781.

25 K. Valegård, L. Liljas, K. Fridborg and T. Unge, *Nature*, 1990, **345**, 36–41.

26 O. Akhavan, M. Choobtashani and E. Ghaderi, *J. Phys. Chem. C*, 2012, **116**, 9653–9659.

27 J. L. Elechiguerra, J. L. Burt, J. R. Morones, A. Camacho-Bragado, X. Gao, H. H. Lara and M. J. Yacaman, *J. Nanobiotechnol.*, 2005, **3**, 1–10.

28 L. Liu, J. Liu, Y. Wang, X. Yan and D. D. Sun, *New J. Chem.*, 2011, **35**, 1418–1423.

29 S. Jaworski, M. Wierzbicki, E. Sawosz, A. Jung, G. Gielerak, J. Biernat, H. Jaremek, W. Łojkowski, B. Woźniak, J. Wojnarowicz, L. Stobiński, A. Małolepszy, M. Mazurkiewicz-Pawlicka, M. Łojkowski, N. Kurantowicz and A. Chwalibog, *Nanoscale Res. Lett.*, 2018, **13**, 116.
30 Y. N. Chen, Y. H. Hsueh, C. Te Hsieh, D. Y. Tzou and P. L. Chang, *Int. J. Environ. Res. Public Health*, 2016, **4**, 4–6, DOI: 10.3390/ijerph13040430.
31 T. Du, J. Lu, L. Liu, N. Dong, L. Fang, S. Xiao and H. Han, *ACS Appl. Bio Mater.*, 2018, **1**, 1286–1293.
32 B. Ziem, J. Rahn, I. Donskyi, K. Silberreis, L. Cuellar, J. Dernedde, G. Keil, T. C. Mettenleiter and R. Haag, *Macromol. Biosci.*, 2017, **17**, 1–9.
33 X. X. Yang, C. M. Li, Y. F. Li, J. Wang and C. Z. Huang, *Nanoscale*, 2017, **9**, 16086–16092.
34 I. S. Donskyi, W. Azab, J. L. Cuellar-Camacho, G. Guday, A. Lippitz, W. E. S. Unger, K. Osterrieder, M. Adeli and R. Haag, *Nanoscale*, 2019, **11**, 15804–15809.
35 M. F. Gholami, D. Lauster, K. Ludwig, J. Storm, B. Ziem, N. Severin, C. Böttcher, J. P. Rabe, A. Herrmann, M. Adeli and R. Haag, *Adv. Funct. Mater.*, 2017, **27**, 1–12.
36 N. K. Rathinam, C. Saravanan, P. Parimal, V. Perumal and M. Perumal, *Korean J. Chem. Eng.*, 2014, **31**, 744–747.
37 X. Du, R. Xiao, H. Fu, Z. Yuan, W. Zhang, L. Yin, C. He, C. Li, J. Zhou, G. Liu, G. Shu and Z. Chen, *Mater. Sci. Eng. C*, 2019, **105**, 110052.
38 A. R. Deokar, A. P. Nagvenkar, I. Kalt, L. Shani, Y. Yeshurun, A. Gedanken and R. Sarid, *Bioconjugate Chem.*, 2017, **28**, 1115–1122.
39 M. C. Wu, A. R. Deokar, J. H. Liao, P. Y. Shih and Y. C. Ling, *ACS Nano*, 2013, **7**, 1281–1290.
40 J. Ge, M. Lan, B. Zhou, W. Liu, L. Guo, H. Wang, Q. Jia, G. Niu, X. Huang, H. Zhou, X. Meng, P. Wang, C. S. Lee, W. Zhang and X. Han, *Nat. Commun.*, 2014, **5**, 1–8.
41 P. Innocenzi, L. Malfatti and D. Carboni, *Nanoscale*, 2015, **7**, 12759–12772.
42 C. M. Carbonaro, R. Corpino, M. Salis, F. Mocci, S. V. Thakkar, C. Olla and P. C. Ricci, *C—Journal of Carbon Research*, 2019, **5**, 60.
43 A. Sharma and J. Das, *J. Nanobiotechnol.*, 2019, **17**, 1–24.
44 R. Ludmerczki, S. Mura, C. M. Carbonaro, I. M. Mandity, M. Carraro, N. Senes, S. Garroni, G. Granozzi, L. Calvillo, S. Marras, L. Malfatti and P. Innocenzi, *Chem.–Eur. J.*, 2019, **25**, 11963–11974.
45 K. Suzuki, L. Malfatti, M. Takahashi, D. Carboni, F. Messina, Y. Tokudome, M. Takemoto and P. Innocenzi, *Sci. Rep.*, 2017, **7**, 1–11.
46 T. Tong, H. Hu, J. Zhou, S. Deng, X. Zhang, W. Tang, L. Fang, S. Xiao and J. Liang, *Small*, 2020, **16**, 1–12.
47 M. Khanal, A. Barras, T. Vausselin, L. Fénéant, R. Boukherroub, A. Siriwardena, J. Dubuisson and S. Szunerits, *Nanoscale*, 2015, **7**, 1392–1402.
48 A. Barras, Q. Pagneux, F. Sane, Q. Wang, R. Boukherroub, D. Hober and S. Szunerits, *ACS Appl. Mater. Interfaces*, 2016, **8**, 9004–9013.
49 M. Z. Fahmi, W. Sukmayani, S. Q. Khairunisa, a. M. Witaningrum, D. W. Indriati, M. Q. Y. Matondang, J. Y. Chang, T. Kotaki and M. Kameoka, *RSC Adv.*, 2016, **6**, 92996–93002.
50 T. Du, J. Liang, N. Dong, L. Liu, L. Fang, S. Xiao and H. Han, *Carbon*, 2016, **110**, 278–285.
51 C. J. Lin, L. Chang, H. W. Chu, H. J. Lin, P. C. Chang, R. Y. L. Wang, B. Unnikrishnan, J. Y. Mao, S. Y. Chen and C. C. Huang, *Small*, 2019, **15**, 1–14.
52 D. Ting, N. Dong, L. Fang, J. Lu, J. Bi, S. Xiao and H. Han, *ACS Appl. Nano Mater.*, 2018, **1**, 5451–5459.
53 A. Łoczechin, K. Séron, A. Barras, E. Giovanelli, S. Belouzard, Y. T. Chen, N. Metzler-Nolte, R. Boukherroub, J. Dubuisson and S. Szunerits, *ACS Appl. Mater. Interfaces*, 2019, **11**, 42964–42974.
54 S. Huang, J. Gu, J. Ye, B. Fang, S. Wan, C. Wang, U. Ashraf, Q. Li, X. Wang, L. Shao, Y. Song, X. Zheng, F. Cao and S. Cao, *J. Colloid Interface Sci.*, 2019, **542**, 198–206.
55 X. Dong, M. M. Moyer, F. Yang, Y. P. Sun and L. Yang, *Sci. Rep.*, 2017, **7**, 1–10.
56 K. Joshi, B. Mazumder, P. Chattopadhyay, N. S. Bora, D. Goyary and S. Karmakar, *Curr. Drug Deliv.*, 2018, **16**, 195–214.
57 M. Li, T. Chen, J. J. Gooding and J. Liu, *ACS Sens.*, 2019, **4**, 1732–1748.
58 Y. Yan, J. Gong, J. Chen, Z. Zeng, W. Huang, K. Pu, J. Liu and P. Chen, *Adv. Mater.*, 2019, **31**, 1–22.
59 S. Tajik, Z. Dourandish, K. Zhang, H. Beitollahi, Q. Van Le, H. W. Jang and M. Shokouhimehr, *RSC Adv.*, 2020, **10**, 15406–15429.
60 S. Zhu, Q. Meng, L. Wang, J. Zhang, Y. Song, H. Jin, K. Zhang, H. Sun, H. Wang and B. Yang, *Angew. Chem. Int. Ed.*, 2013, **52**, 3953–3957.
61 K. Ghanbari, M. Roushani and A. Azadbakht, *Anal. Biochem.*, 2017, **534**, 64–69.
62 Q. Xiang, J. Huang, H. Huang, W. Mao and Z. Ye, *RSC Adv.*, 2018, **8**, 1820–1825.
63 M. L. Chen, Y. J. He, X. W. Chen and J. H. Wang, *Bioconjugate Chem.*, 2013, **24**, 387–397.
64 D. Iannazzo, A. Pistone, S. Ferro, L. De Luca, A. M. Monforte, R. Romeo, M. R. Buemi and C. Pannecouque, *Bioconjugate Chem.*, 2018, **29**, 3084–3093.
65 J. Du, B. Feng, Y. Dong, M. Zhao and X. Yang, *Nanoscale*, 2020, **12**, 9219–9230.
66 M. Prato, *J. Mater. Chem.*, 1997, **7**, 1097–1109.
67 R. Sijbesma, G. Srdanov, F. Wudl, J. A. Castoro, C. Wilkins, S. H. Friedman, D. L. Decamp and G. L. Kenyonl, *J. Am. Chem. Soc.*, 1993, **115**, 6510–6512.
68 E. Castro, Z. S. Martinez, C. S. Seong, A. Cabrera-Espinoza, M. Ruiz, A. Hernandez Garcia, F. Valdez, M. Llano and L. Echegoyen, *J. Med. Chem.*, 2016, **59**, 10963–10973.
69 G. Luca Marcorin, T. Da Ros, S. Castellano, G. Stefancich, I. Bonin, S. Miertus and M. Prato, *Org. Lett.*, 2000, **2**, 3955–3957.
70 A. Barzegar, S. Jafari Mousavi, H. Hamidi and M. Sadeghi, *Phys. E Low-dimens. Syst. Nanostruct.*, 2017, **93**, 324–331.
71 Z. S. Martinez, E. Castro, C. S. Seong, M. R. Cerón, L. Echegoyen and M. Llano, *Antimicrob. Agents Chemother.*, 2016, **60**, 5731–5741.

72 H. Yilmaz, L. Ahmed, B. Rasulev and J. Leszczynski, *J. Nanoparticle Res.*, 2016, **18**, 123.
73 N. a. Saleh, *Spectrochim. Acta Mol. Biomol. Spectrosc.*, 2015, **136**, 1523–1529.
74 K. A. Khadra, S. Mizyed, D. Marji, S. F. Haddad, M. Ashram and A. Foudeh, *Spectrochim. Acta Mol. Biomol. Spectrosc.*, 2015, **136**, 1869–1874.
75 S. Marchesan, T. Da Ros, G. Spalluto, J. Balzarini and M. Prato, *Bioorg. Med. Chem. Lett*, 2005, **15**, 3615–3618.
76 S. Promsri, P. Chuichay, V. Sanghiran, V. Parasuk and S. Hannongbua, *J. Mol. Struct.: THEOCHEM*, 2005, **715**, 47–53.
77 J. Nacsa, J. Segesdi, Á. Gyuris, T. Braun, H. Rausch, Á. Buvári-Barcza, L. Barcza, J. Minarovits and J. Molnár, *Fullerene Sci. Technol.*, 1997, **5**, 969–976.
78 R. F. Rhule, J. T. Hill, C. L. Zheng and Z. Schinazi, in *Metallopharmaceuticals II. Topics in Biological Inorganic Chemistry*, Springer Berlin Heidelberg, 1999, vol. 2, pp. 117–137.
79 E. Nakamura and H. Isobe, *Acc. Chem. Res.*, 2003, **36**, 807–815.
80 O. a. Troshina, P. a. Troshin, A. S. Peregudov, V. I. Kozlovskiy, J. Balzarini and R. N. Lyubovskaya, *Org. Biomol. Chem.*, 2007, **5**, 2783–2791.
81 A. B. Kornev, A. S. Peregudov, V. M. Martynenko, J. Balzarini, B. Hoorelbeke and P. a. Troshin, *Chem. Commun.*, 2011, **47**, 8298–8300.
82 H. Kataoka, T. Ohe, K. Takahashi, S. Nakamura and T. Mashino, *Bioorg. Med. Chem. Lett*, 2016, **26**, 4565–4567.
83 I. N. Falynskova, K. S. Ionova, a. V. Dedova, I. a. Leneva, N. R. Makhmudova and L. D. Rasnetsov, *Pharm. Chem. J.*, 2014, **48**, 85–88.
84 N. E. Fedorova, R. R. Klimova, Y. a. Tulenev, E. V. Chichev, A. B. Kornev, P. a. Troshin and A. a. Kushch, *Mendeleev Commun.*, 2012, **22**, 254–256.
85 J. Ramos-Soriano, J. J. Reina, B. M. Illescas, N. De La Cruz, L. Rodríguez-Pérez, F. Lasala, J. Rojo, R. Delgado and N. Martín, *J. Am. Chem. Soc.*, 2019, **141**, 15403–15412.
86 J. W. Arbogast, A. P. Darmanyan, C. S. Foote, Y. Rubin, F. N. Diederich, M. M. Alvarez, S. J. Anz and R. L. Whetten, *J. Phys. Chem.*, 1991, **95**, 11–12.
87 D. R. Kearns, *Chem. Rev.*, 1971, **71**, 395–427.
88 I. V. Bagrov, I. M. Belousova, V. M. Kiselev and I. M. Kislyakov, *J. Opt. Technol.*, 2019, **86**, 66.
89 L. Brunet, D. Y. Lyon, E. M. Hotze, P. J. J. Alvarez and M. R. Wiesner, *Environ. Sci. Technol.*, 2009, **43**, 4355–4360.
90 J. Lee, S. Hong, Y. MacKeyev, C. Lee, E. Chung, L. J. Wilson, J. H. Kim and P. J. J. Alvarez, *Environ. Sci. Technol.*, 2011, **45**, 10598–10604.
91 J. Lenard and R. Vanderoef, *Photochem. Photobiol.*, 1993, **58**, 527–531.
92 F. Käsermann and C. Kempf, *Antiviral Res.*, 1997, **34**, 65–70.
93 F. Käsermann and C. Kempf, *Rev. Med. Virol.*, 1998, **8**, 143–151.
94 Y. Rud, S. Prylutska, L. Buchatskyy, Y. Prylutskyy, U. Ritter and P. Scharff, *Materwiss. Werksttech.*, 2011, **42**, 136–138.
95 V. V. Zarubaev, I. M. Belousova, O. I. Kiselev, L. B. Piotrovsky, P. M. Anfimov, T. C. Krisko, T. D. Muraviova, V. V. Rylkov, A. M. Starodubzev and A. C. Sirotkin, *Photodiagnosis Photodyn. Ther.*, 2007, **4**, 31–35.
96 A. R. Badireddy, J. F. Budarz, S. Chellam and M. R. Wiesner, *Environ. Sci. Technol.*, 2012, **46**, 5963–5970.
97 I. M. Belousova, I. M. Kislyakov, T. D. Muraviova, a. M. Starodubtsev, T. K. Kris'ko, E. a. Selivanov, N. P. Sivakova, I. S. Golovanova, S. D. Volkova, a. a. Shtro and V. V. Zarubaev, *Photodiagnosis Photodyn. Ther.*, 2014, **11**, 165–170.
98 M. Cho, J. Lee, Y. MacKeyev, L. J. Wilson, P. J. J. Alvarez, J. B. Hughes and J. H. Kim, *Environ. Sci. Technol.*, 2010, **44**, 6685–6691.
99 S. D. Snow, K. Park and J. H. Kim, *Environ. Sci. Technol. Lett.*, 2014, **1**, 290–294.
100 J. Kim, H. Lee, J. Y. Lee, K. H. Park, W. Kim, J. H. Lee, H. J. Kang, S. W. Hong, H. J. Park, S. Lee, J. H. Lee, H. D. Park, J. Y. Kim, Y. W. Jeong and J. Lee, *Appl. Catal., B*, 2020, **270**, 118862.
101 A. Pinna, L. Malfatti, M. Piccinini, P. Falcaro and P. Innocenzi, *J. Synchrotron Radiat.*, 2012, **19**, 586–590.
102 L. Chen and J. Liang, *Mater. Sci. Eng. C*, 2020, **112**, 110924.
103 K. Turcheniuk and V. N. Mochalin, *Nanotechnology*, DOI: 10.1088/1361-6528/aa6ae4.
104 A. M. Schrand, S. A. C. Hens and O. a. Shenderova, *Crit. Rev. Solid State Mater. Sci.*, 2009, **34**, 18–74.
105 L. Wang, Z. Yuan, H. E. Karahan, Y. Wang, X. Sui, F. Liu and Y. Chen, *Nanoscale*, 2019, **11**, 9819–9839.
106 S. J. Yu, M. W. Kang, H. C. Chang, K. M. Chen and Y. C. Yu, *J. Am. Chem. Soc.*, 2005, **127**, 17604–17605.
107 J. T. Paci, H. B. Man, B. Saha, D. Ho and G. C. Schatz, *J. Phys. Chem. C*, 2013, **117**, 17256–17267.
108 D. Mitev, R. Dimitrova, M. Spassova, C. Minchev and S. Stavrev, *Diamond Relat. Mater.*, 2007, **16**, 776–780.
109 I. Petrov, O. Shenderova, V. Grishko, V. Grichko, T. Tyler, G. Cunningham and G. McGuire, *Diamond Relat. Mater.*, 2007, **16**, 2098–2103.
110 V. T. Ivanova, M. V. Ivanova, B. V. Spitsyn, K. O. Garina, S. V. Trushakova, a. a. Manykin, a. P. Korzhenevsky and E. I. Burseva, *J. Phys.: Conf. Ser.*, 2012, **345**, 012019.